C_4-Ring Ligand-transfer Reactions: Applications to Cluster Chemistry. Crystal Structures of $[Ru_5C(CO)_{13}(\eta\text{-}C_4Ph_4)]$ and $[Ru_6C(CO)_{15}(\eta\text{-}C_4Ph_4)]$†

Paul J. Dyson,[a] Scott L. Ingham,[b] Brian F. G. Johnson,*[,b] John E. McGrady,[a] D. Michael P. Mingos*[,a] and Alexander J. Blake[b]

[a] *Department of Chemistry, Imperial College of Science, Technology and Medicine, South Kensington, London SW7 2AY, UK*

[b] *Department of Chemistry, The University of Edinburgh, West Mains Road, Edinburgh EH9 3JJ, UK*

Redox-mediated ligand-transfer reactions between the cationic complex $[Pd(\eta\text{-}C_4Ph_4)(Me_2CO)_2]^{2+}$ and the dianionic clusters, $[Ru_5C(CO)_{14}]^{2-}$ and $[Ru_6C(CO)_{16}]^{2-}$ afforded $[Ru_5C(CO)_{13}(\eta\text{-}C_4Ph_4)]$ **1** and $[Ru_6C(CO)_{15}(\eta\text{-}C_4Ph_4)]$ **2**, respectively. The new clusters **1** and **2** have been characterised by spectroscopic techniques in solution and in the solid-state by single-crystal X-ray diffraction. In **1** the ring is co-ordinated to a basal ruthenium atom of the square-pyramidal cluster framework, while in **2** the octahedral metal core of the parent complex has opened slightly through the elongation of one Ru–Ru bond. The reasons for this structural change have been analysed using extended-Hückel molecular-orbital calculations.

The first examples of cyclobutadiene ligand transfer reactions were reported in 1963 and involved $[\{Pd(\eta\text{-}C_4Ph_4)Br\}_2]$ with either $Fe(CO)_5$ or $Ni(CO)_4$ and yielded $[Fe(CO)_3(\eta\text{-}C_4Ph_4)]$ and $[\{Ni(\eta\text{-}C_4Ph_4)Br_2\}_2]$, respectively.[1] Since that initial report, detailed studies of this class of reaction have been made and a diverse chemistry has been observed.[2] In cluster chemistry it was found that the reaction of the palladium complex with triruthenium dodecacarbonyl, $[Ru_3(CO)_{12}]$, gave the monoruthenium complex $[Ru(CO)_3(\eta\text{-}C_4Ph_4)]$ rather than a cluster compound.[2]

In more recent years, one of our objectives has been to synthesise and characterise a wide range of clusters bearing unsaturated ring systems, and this has resulted in the development of a diverse array of synthetic techniques.[3] Clusters with co-ordinated homocyclic rings with between five and eight carbon atoms are plentiful, and the rings display a remarkable variation in the bonding types they exhibit. Clusters containing the cyclobutadiene unit were unknown until recently, when we reported the synthesis and characterisation of $[Ru_5C(CO)_{13}(\eta\text{-}C_4Ph_4)]$ **1**.[4]

In this paper we provide a detailed account of the synthetic methods which give easy access to a range of cyclobutadiene clusters.‡ We have found that the traditional ligand-transfer reaction described above is not effective when applied to cluster molecules, but a modification of this route, which takes into account the redox nature of the clusters has proved successful. Suitable dianionic clusters react directly with a dicationic cyclobutadiene complex cation presumed to be $[Pd(\eta\text{-}C_4Ph_4)(Me_2CO)_2]^{2+}$, to give $[Ru_5C(CO)_{13}(\eta\text{-}C_4Ph_4)]$ **1** and $[Ru_6C(CO)_{15}(\eta\text{-}C_4Ph_4)]$ **2** in high yield.

Results and Discussion

The cyclobutadiene-palladium complexes $[\{Pd(\eta\text{-}C_4R_4)Cl\}_2]$ may be prepared in high yield from the reaction between the appropriate acetylene (RC_2R'; R = Ph, R' = Ph or Me) and $[PdCl_2(PhCN)_2]$.[5] The complex, $[\{Pd(\eta\text{-}C_4Ph_4)Cl\}_2]$, reacts with 2 equivalents of $AgBF_4$ in acetone resulting in the formation of the highly reactive solvated species $[Pd(\eta\text{-}C_4Ph_4)(Me_2CO)_3][BF_4]_2$. The reaction mixture was filtered in order to remove AgCl which precipitates during the process, and the resulting bright yellow filtrate was reduced to dryness affording a yellow-brown solid. This solid was redissolved in dichloromethane, heated under reflux, and an equimolar equivalent of the appropriate cluster dianion, *viz.* $[N(PPh_3)_2][Ru_5C(CO)_{14}]$ or $[N(PPh_3)_2][Ru_6C(CO)_{16}]$, added dropwise over 10 min and stirred at reflux temperature for a short while thereafter. Both reactions give one major dark brown product which may be purified by filtration of the post-reaction mixture through a short column containing silica gel.

In the case of the pentanuclear dianionic cluster, $[Ru_5C(CO)_{14}]^{2-}$, the dark brown product undergoes quantitative conversion to a second species on standing in dichloromethane at room temperature for 24 h. The infrared spectrum ($\tilde{\nu}_{CO}/cm^{-1}$, recorded in CH_2Cl_2) of the initial compound exhibits carbonyl stretching modes at 2060vs and 2027s cm^{-1}. After standing for 24 h, the spectrum contains peaks at 2080m, 2060s (sh), 2046vs, 2028s (sh), 1967w (br), 1906w (br) and 1792vw (br) cm^{-1}. This latter complex has been fully characterised by spectroscopy and a single-crystal X-ray diffraction analysis as $[Ru_5C(CO)_{13}(\eta\text{-}C_4Ph_4)]$ **1** (see below). We believe the former complex consists of a hexanuclear cluster involving the $Ru_5C(CO)_{14}$ unit where the square face has been partially capped by the palladium–cyclobutadiene fragment, *i.e.* $[Ru_5PdC(CO)_{14}(\eta\text{-}C_4Ph_4)]$. A well established reaction of $[Ru_5C(CO)_{14}]^{2-}$ involves capping with the ruthenium–benzene unit, $[Ru(\eta\text{-}C_6H_6)]^{2+}$, giving the stable octahedral cluster $[Ru_6C(CO)_{14}(\eta\text{-}C_6H_6)]$.[6] The IR spectrum of this species is slightly different from that of the proposed Ru_5Pd cluster, the difference probably arising because the Pd unit caps only one or two edges of the square base. Although the precise method by which the C_4Ph_4 ring undergoes transfer from the Pd atom to a basal Ru atom is uncertain, the process necessarily involves both the oxidation of the cluster dianion and the expulsion of

† *Supplementary data available:* see Instructions for Authors, *J. Chem. Soc., Dalton Trans.*, 1995, Issue 1, pp. xxv–xxx.

Non-SI unit employed: eV ≈ 1.60 × 10^{-19} J.

‡ Preliminary results from studies conducted with dianionic high nuclearity osmium clusters indicate that a similar reaction takes place with $[Pd(\eta\text{-}C_4Ph_4)(Me_2CO)_2][BF_4]_2$.

one carbonyl group. In addition, Pd^{2+} is reduced to metallic palladium which has been identified in the reaction mixture. This sequence of events involving the transfer of the ligand may be facilitated by a polyhedral rearrangement of the cluster framework from the familiar square-based pyramid to a bridged-butterfly geometry with the C_4 unit attached to the bridging Ru atom. This intermediate complex would have the same number of CO ligands as the starting material and subsequent elimination of one CO (thereby giving the number found in the product) would result in the regeneration of the original cluster polyhedron. This diamond–square–diamond mechanism dominates the chemistry of the pentaruthenium cluster compounds.[7] With the hexaruthenium system, no intermediate species has been identified, and only $[Ru_6C(CO)_{15}(\eta\text{-}C_4Ph_4)]$ **2** is observed. This is not entirely unexpected since there is no ideal capping site present similar to the square base in the Ru_5C system. The palladium complex is still believed to attach itself to the cluster forming a heptanuclear species, but the actual transfer of the C_4Ph_4 ligand must occur at a faster rate due to the instability of the heptanuclear complex. In a similar reaction between $[Ru(\eta\text{-}C_6H_6)(MeCN)_3]^{2+}$ and the hexanuclear benzene cluster dianion, $[Ru_6C(CO)_{13}(\eta\text{-}C_6H_6)]^{2-}$, the bis(benzene) cluster $[Ru_6C(CO)_{13}(\eta\text{-}C_6H_6)(\mu_3\text{-}C_6H_6)]$ is formed rather than a heptanuclear derivative. There is a connection between these two reactions, although significantly, the palladium and ruthenium complexes react in quite different ways with the pentaruthenium cluster.

Spectroscopic and Solid-state Characterisation of Clusters **1** *and* **2**.—The mass spectrum of **1** and **2** contain strong molecular ions at *m/z* 1237 (Calc. 1238) and 1395 (Calc. 1395), respectively, together with subsequent ions consistent with masses corresponding to the sequential loss of 13 and 15 carbonyl groups for **1** and **2**, respectively. The ^1H NMR spectra of **1** and **2**, recorded in $CDCl_3$, exhibit multiplet resonances in the range δ 7.12–7.94 and 6.93–7.98, respectively, which may be assigned to the protons of the phenyl groups attached to the C_4 core. No signals from metal hydrides were observed between δ 30 and −30.

Crystals of **1** suitable for an X-ray diffraction analysis were grown from a solution of dichloromethane–octane by slow evaporation. The molecular structure of **1** is depicted in Fig. 1 together with relevant bond parameters. The ruthenium atoms form a square-based pyramidal geometry, similar to that found in the parent cluster, $[Ru_5C(CO)_{15}]$, but somewhat less regular,[8] probably due to the presence of the C_4Ph_4 ligand. The Ru–Ru bond lengths range from 2.790(2) to 2.948(2) Å [mean 2.85 Å] {[*cf.* $[Ru_5C(CO)_{15}]$, range 2.800(2)–2.882(2) Å, mean 2.84 Å]} and those distances involving the Ru carrying the C_4Ph_4 ligand are longer than the remaining Ru–Ru contacts (mean 2.88 *vs.* 2.83 Å, respectively) despite two of these edges being bridged by carbonyl ligands. The Ru–C(carbide) distances do not show much variation within the square base, ranging from 2.012(9) to 2.059(9) Å, but the interaction with the apical ruthenium atom [Ru(5)] is weaker [2.254(10) Å], so that the carbide is displaced out of the basal plane by 0.251 Å. The most important feature of compound **1** is the presence of the C_4Ph_4 group which is η^4 bonded to a basal metal atom [Ru(1)–C(1L) 2.239(9), Ru(1)–C(2L) 2.202(9), Ru(1)–C(3L)

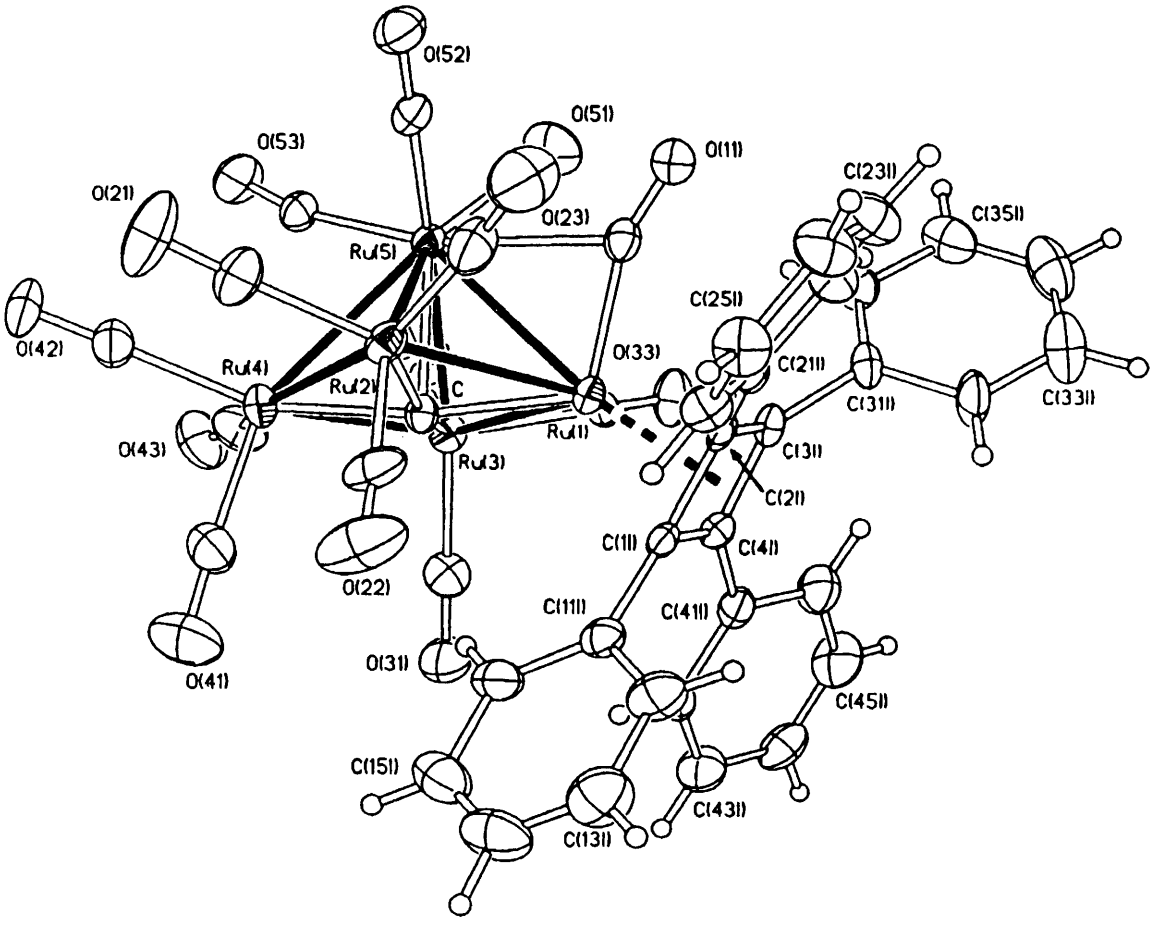

Fig. 1 The molecular structure of $[Ru_5C(CO)_{13}(\eta\text{-}C_4Ph_4)]$ **1** in the solid state depicted with 30% thermal ellipsoids. Principal bond parameters (Å) include: Ru–Ru, Ru(1)–Ru(2) 2.948(2), Ru(1)–Ru(3) 2.8319(14), Ru(1)–Ru(5) 2.862(2), Ru(2)–Ru(4) 2.831(2), Ru(2)–Ru(5) 2.803(2), Ru(3)–Ru(4) 2.790(2), Ru(3)–Ru(5) 2.8026(14), Ru(4)–Ru(5) 2.898(2); $Ru\text{–}C_{carbide}$, Ru(1)–C 2.025(9), Ru(2)–C 2.026(9), Ru(3)–C 2.059(9), Ru(4)–C 2.012(9), Ru(5)–C 2.254(10); $Ru(1)\text{–}C_{ring}$, Ru(1)–C(1L) 2.239(9), Ru(1)–C(2L) 2.202(9), Ru(1)–C(3L) 2.193(9), Ru(1)–C(4L) 2.271(10); $C_{ring}\text{–}C_{ring}$, C(1L)–C(2L) 1.491(13), C(2L)–C(3L) 1.467(13), C(3L)–C(4L) 1.468(14), C(4L)–C(1L) 1.460(14)

2.193(9), Ru(1)–C(4L) 2.271(10) Å]. Within the C_4-square, the mean C–C bond length is 1.47 Å, which is typical of those found in four-membered ring systems. The four phenyl groups (1, 2, 3 and 4) exhibit dihedral angles of 60, 15, 82 and 21° respectively, thus alternate rings show similar degrees of torsion, two being relatively flat and two almost perpendicular to the square plane. The phenyl groups also bend out of the square plane away from the cluster, the mean elevation of the *ipso*-carbon atoms above this plane being 0.33 Å. The presence of the cyclobutadiene ring alters the topology of the carbonyl groups with respect to the parent cluster, which range from terminal groups to bridging ligands so as to give essentially a homogeneous electron distribution.

Crystals of **2** used in the X-ray structure determination were also grown from a solution of dichloromethane–octane by slow evaporation. The molecular structure of **2** is illustrated in Fig. 2 together with relevant bond parameters. The six ruthenium atoms adopt an octahedral geometry although one of the Ru–Ru edges involving the Ru atom to which the cyclobutadiene ligand is bonded is longer than the distance which is generally considered to constitute a bond [Ru(5)–Ru(6) 3.213 Å]. Excluding this distance, the mean Ru–Ru bond length is 2.8818(12) Å [with lengths ranging from 2.8276(8) to 2.9676(12) Å]. The lengthening of the Ru(5)–Ru(6) contact is also reflected in the angle formed with the carbide atom [Ru(5)–C–Ru(6) 104.35(2)°] which is considerably larger than that normally observed, *i.e.* ≈90°. The carbide atom is displaced from the centre of the cavity so that it is positioned closer to the four Ru atoms involved in open face [Ru(1)Ru(2)Ru(5)Ru(6), mean 2.037(3) Å] and further from the other two Ru atoms [mean 2.119(3) Å] possibly reflecting an electronic compensatory effect. The co-ordination of the carbonyl ligands ranges from bridging to terminal as observed in **1** and the parent cluster $[Ru_6C(CO)_{17}]$. Three bridging carbonyls are wrapped around the molecular equator of the cluster [*viz.* Ru(5)Ru(4)Ru(3)Ru(6)] and each of these metals also have two terminal carbonyl groups except for Ru(5) to which the C_4Ph_4 ring is co-ordinated. Three terminal carbonyl ligands co-ordinate to Ru(1) and Ru(2). The C_4Ph_4 group in **2** is η^4 bonded to Ru(5) in a similar fashion to that observed in **1** [Ru(5)–C(1L) 2.178(3), Ru(5)–C(2L) 2.221(3), Ru(5)–C(3L) 2.192(3), Ru(5)–C(4L) 2.195(3) Å, mean C–C bond length 1.470(4) Å]. The four phenyl groups exhibit a similar geometry with dihedral angles of 55, 22, 79 and 25° for 1, 2, 3 and 4, respectively, with a mean elevation of the *ipso*-carbon atoms above the C_4 ring plane of 0.31 Å.

Extended-Hückel Molecular-orbital Calculations for **2** *and* $[Ru_6C(CO)_{17}]$.—Due to the rather unusual Ru–Ru contact in $[Ru_6C(CO)_{15}(\eta\text{-}C_4Ph_4)]$ **2** (see above), extended-Hückel calculations were used to compare the structures of **2** and the related binary carbonyl cluster $[Ru_6C(CO)_{17}]$, which has recently been characterised in the solid-state.[9] It should be noted that two different polymorphic modifications of $[Ru_6C(CO)_{17}]$ have been established. The two forms differ in the relative orientation of the axial $Ru(CO)_3$ groups: in one they

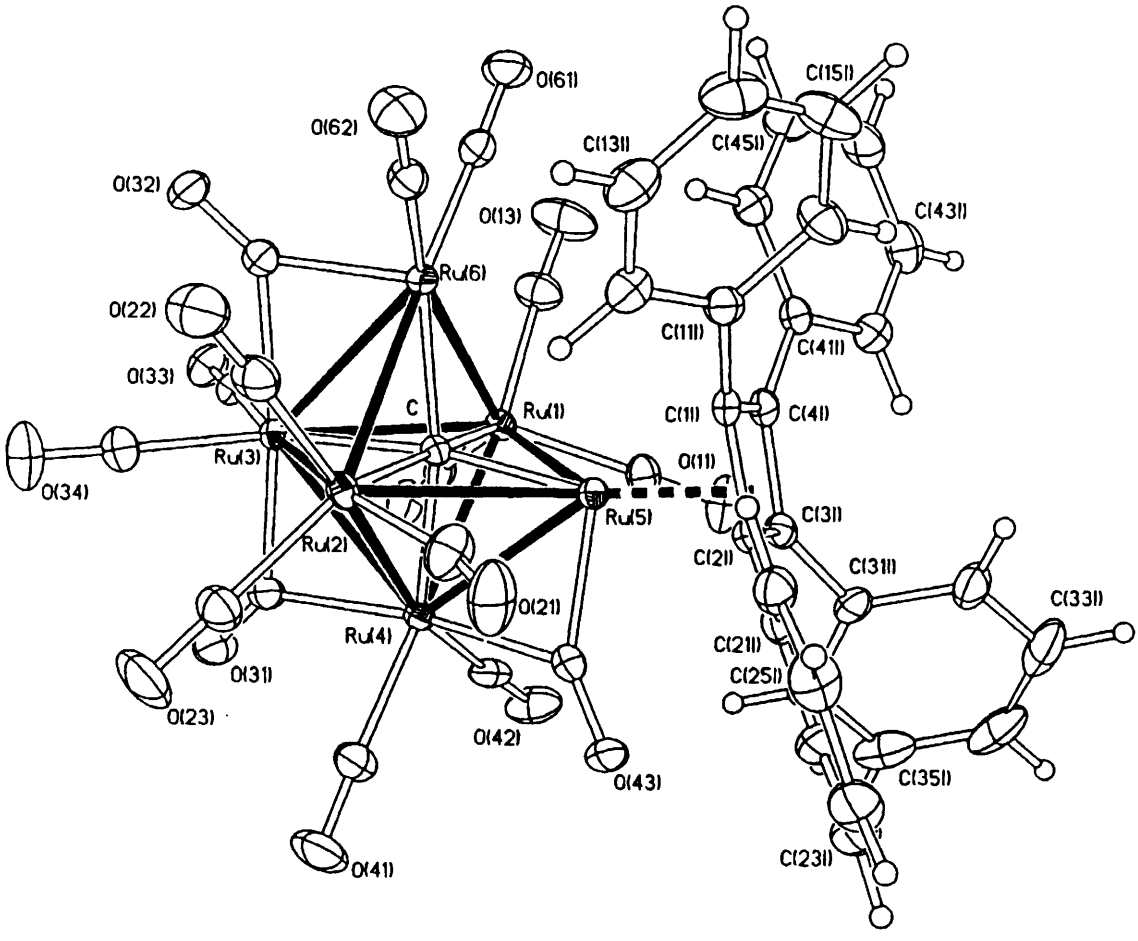

Fig. 2 The molecular structure of $[Ru_6C(CO)_{15}(\eta\text{-}C_4Ph_4)]$ **2** in the solid state depicted with 50% thermal ellipsoids. Principal bond parameters (Å) include: Ru–Ru, Ru(1)–Ru(3) 2.8685(11), Ru(1)–Ru(4) 2.8369(9), Ru(1)–Ru(5) 2.9619(12), Ru(1)–Ru(6) 2.9344(10), Ru(2)–Ru(3) 2.8518(12), Ru(2)–Ru(4) 2.8585(9), Ru(2)–Ru(5) 2.9676(12), Ru(2)–Ru(6) 2.9286(10), Ru(3)–Ru(4) 2.8315(10), Ru(3)–Ru(6) 2.8276(8), Ru(4)–Ru(5) 2.8327(8), Ru(5) ··· Ru(6) 3.213; Ru–$C_{carbide}$, Ru(1)–C 2.038(3), Ru(2)–C 2.041(3), Ru(3)–C 2.148(3), Ru(4)–C 2.089(3), Ru(5)–C 2.033(3), Ru(6)–C 2.034(3); Ru(5)–C_{ring}, Ru(5)–C(1L) 2.178(3), Ru(5)–C(2L) 2.221(3), Ru(5)–C(3L) 2.192(3), Ru(5)–C(4L) 2.195(3); C_{ring}–C_{ring}, C(1L)–C(2L) 1.475(4), C(2L)–C(3L) 1.472(4), C(3L)–C(4L) 1.454(4), C(4L)–C(1L) 1.463(4)

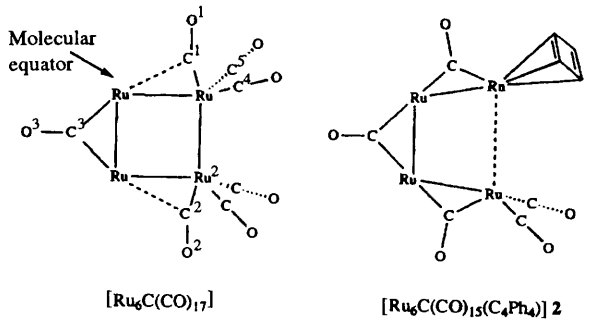

Fig. 3 Molecular structure of $[Ru_6C(CO)_{17}]$ and $[Ru_6C(CO)_{15}(\eta\text{-}C_4Ph_4)]$ **2** in the equatorial plane

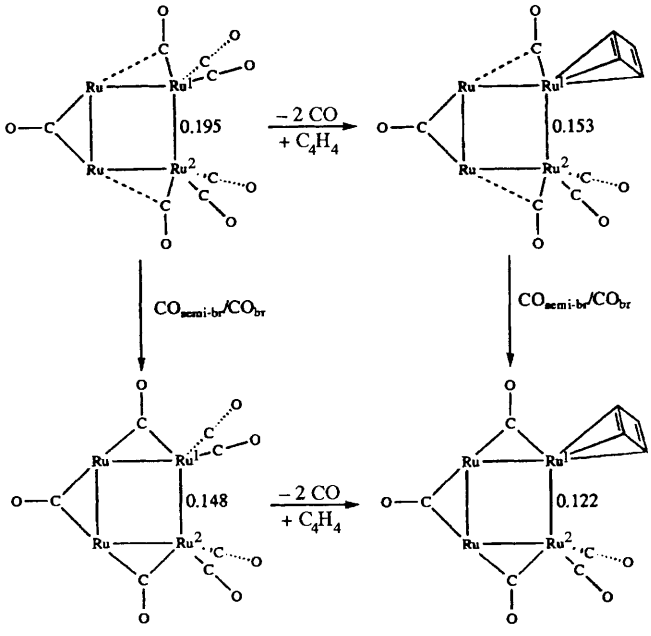

Fig. 4 Changes in Ru–Ru reduced overlap population during the transformation from $[Ru_6C(CO)_{17}]$ to $[Ru_6C(CO)_{15}(\eta\text{-}C_4Ph_4)]$ **2**

are eclipsed and in the other staggered. The eclipsed form of $[Ru_6C(CO)_{17}]$ was used for the calculations because of its similarity to **2**. The molecular equators in $[Ru_6C(CO)_{17}]$ and **2** are compared in Fig. 3. Apart from the longer Ru^1–Ru^2 bond length in the latter, the positions of the carbonyls C^1O and C^2O differ, and move from semi-bridging positions in $[Ru_6C(CO)_{17}]$ to almost symmetrical bridging sites in **2**.

In order to identify the factors which cause the elongation of the Ru–Ru bond in **2**, two of the carbonyl groups (C^4O and C^5O) in $[Ru_6C(CO)_{17}]$ were replaced with a C_4H_4 ligand whilst retaining the semi-bridging geometry of C^1O and C^2O. The carbonyl ligands were then allowed to move to the symmetrically bridged geometry observed in the solid-state structure of **2**. Alternatively, the relationship between $[Ru_6C(CO)_{17}]$ and **2** may be expressed in terms of the carbonyls moving into the bridging position first, followed by the replacement of the two carbonyls by C_4H_4. This mode of analysis is illustrated in Fig. 4. The geometry of the Ru_6 core was restricted to the idealised octahedral geometry throughout, and the computed Ru^1–Ru^2 reduced overlap populations were used to indicate changes in the Ru^1–Ru^2 bond strengths. Full details of the extended-Hückel calculations and the relevant parameters are given in the Experimental section. The resulting computed reduced overlap populations for Ru^1–Ru^2 are summarised in Fig. 4. Populations between the other Ru centres remain relatively unaffected by the structural changes described in Fig. 4. This figure illustrates that both these structural

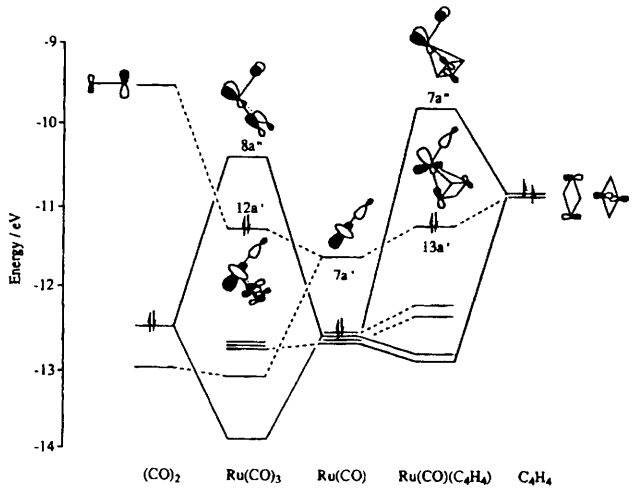

Fig. 5 Interaction of a Ru–CO fragment with $(CO)_2$ and C_4H_4 units

changes (*viz.* substitution of two terminal CO ligands by C_4H_4 and the movement of C^1O and C^2O into bridging positions) result in a significant reduction in the Ru^1–Ru^2 reduced overlap population, and consequently a weakened Ru^1–Ru^2 bond.

The differences in the bonding capabilities of $Ru(CO)_3$ and $Ru(CO)(\eta\text{-}C_4H_4)$ were defined by comparing the interaction of Ru(CO) with $(CO)_2$ and C_4H_4. The relevant interaction diagram is shown in Fig. 5. With the geometry appropriate for semi-bridging CO, the $Ru(CO)_3$ fragment has only C_s symmetry, and the degeneracy of the familiar e frontier orbital set is broken. The highest occupied orbital is the a' component [12a' in $Ru(CO)_3$] while the lowest unoccupied orbital is the a'' component (8a''). Replacement of the two CO ligands by cyclobutadiene rehybridises the 12a' molecular orbital [13a' in $Ru(CO)(\eta\text{-}C_4H_4)$] which consequently is unable to overlap as effectively with an orbital on the Ru atom lying approximately *trans* to the unique carbonyl. The rehybridisation thus effectively lowers the reduced overlap population of the Ru^1–Ru^2 bond when the $Ru(CO)(\eta\text{-}C_4H_4)$ fragment is incorporated into the cluster.

The effect of moving the carbonyl ligands (C^1O and C^2O) into symmetrically bridging positions may be analysed by considering the change in orientation of the 13a' orbital of **2**. As the ligand moves towards a bridging position the orbital is directed increasingly away from the Ru^1–Ru^2 axis, thereby reducing the Ru^1–Ru^2 overlap. While the electronic consequences of the change from semi-bridging to a symmetrically bridging geometry are relatively simple to understand, the underlying cause of the change is less clear. The C_4Ph_4 ligand is considerably more bulky than the two carbonyl groups present in the parent cluster, and in **2**, two of the phenyl ring protons lie within 2.7 Å of the bridging CO ligands. It would seem probable that steric repulsion between the phenyl groups and the equatorial CO ligands results in their preference for bridging positions in **2**. In the pentanuclear system compound **1** does not exhibit any unusual distortions to the metal core, despite the relative ease of transition to a trigonal-bipyramidal structure. This is presumably due to the ability of the C_4Ph_4 ligand to adopt an angled position partially under the square-base of the pyramid in which the phenyl groups experience less repulsion with the metal carbonyls.

Experimental

All reactions were carried out with the exclusion of air using solvents freshly distilled under an atmosphere of nitrogen. Subsequent work-up of products was achieved without precautions to exclude air. IR spectra were recorded on a Perkin-Elmer 1710 series FTIR instrument in CH_2Cl_2 using NaCl cells

Table 1 Atomic coordinates with estimated standard deviations (e.s.d.s) in parentheses for **1**

Atom	*x*	*y*	*z*	Atom	*x*	*y*	*z*
Ru(1)	0.776 70(5)	0.009 66(5)	0.272 37(5)	C(52)	0.635 9(6)	0.113 0(7)	0.077 0(7)
Ru(2)	0.611 93(5)	0.080 05(5)	0.263 18(5)	C(53)	0.584 6(7)	−0.053 5(7)	0.049 2(7)
Ru(3)	0.708 86(5)	−0.144 34(5)	0.210 75(5)	C(1L)	0.813 7(6)	0.025 3(6)	0.411 9(6)
Ru(4)	0.552 53(5)	−0.081 67(6)	0.216 27(6)	C(11L)	0.764 9(6)	0.014 9(6)	0.485 2(7)
Ru(5)	0.668 50(5)	0.003 43(5)	0.119 88(5)	C(12L)	0.783 6(8)	0.062 6(8)	0.559 0(7)
C	0.662 2(6)	−0.035 4(6)	0.256 8(6)	C(13L)	0.738 9(10)	0.054 4(10)	0.630 7(9)
O(11)	0.818 9(5)	0.139 6(6)	0.143 1(5)	C(14L)	0.681 3(10)	−0.003 6(10)	0.628 7(10)
O(21)	0.441 3(6)	0.133 8(7)	0.197 6(7)	C(15L)	0.659 4(8)	−0.053 3(9)	0.558 2(10)
O(22)	0.578 0(7)	0.109 3(7)	0.449 2(6)	C(16L)	0.703 4(7)	−0.044 9(8)	0.485 3(8)
O(23)	0.670 4(7)	0.259 8(6)	0.243 2(7)	C(2L)	0.842 9(5)	0.097 0(6)	0.362 2(6)
O(31)	0.726 2(6)	−0.280 7(6)	0.347 3(6)	C(21L)	0.837 4(6)	0.187 9(6)	0.365 9(6)
O(32)	0.720 0(7)	−0.259 2(6)	0.056 5(7)	C(22L)	0.886 8(7)	0.237 0(7)	0.319 1(7)
O(33)	0.887 5(5)	−0.128 9(5)	0.193 3(5)	C(23L)	0.884 2(8)	0.323 4(8)	0.325 9(8)
O(41)	0.501 0(8)	−0.144 6(8)	0.385 0(7)	C(24L)	0.833 1(8)	0.362 5(7)	0.376 5(8)
O(42)	0.377 8(5)	−0.048 2(7)	0.140 4(6)	C(25L)	0.785 7(7)	0.314 3(8)	0.423 8(8)
O(43)	0.538 5(6)	−0.256 7(6)	0.141 0(7)	C(26L)	0.787 2(7)	0.228 3(7)	0.419 5(6)
O(51)	0.789 1(6)	0.050 5(6)	−0.008 6(6)	C(3L)	0.900 1(6)	0.041 2(6)	0.324 5(6)
O(52)	0.617 0(5)	0.174 3(5)	0.044 4(5)	C(31L)	0.976 4(6)	0.056 5(6)	0.282 4(7)
O(53)	0.545 1(5)	−0.083 7(6)	−0.005 2(5)	C(32L)	1.039 5(7)	0.089 6(8)	0.335 9(8)
C(11)	0.791 5(6)	0.085 8(7)	0.178 2(7)	C(33L)	1.112 0(8)	0.105 9(9)	0.302 1(12)
C(21)	0.504 5(8)	0.111 2(8)	0.221 6(8)	C(34L)	1.121 2(9)	0.089 0(10)	0.216 1(12)
C(22)	0.593 4(8)	0.096 5(8)	0.380 8(8)	C(35L)	1.059 5(8)	0.057 2(8)	0.164 1(9)
C(23)	0.650 1(8)	0.192 0(9)	0.253 4(9)	C(36L)	0.986 9(7)	0.039 3(7)	0.197 3(7)
C(31)	0.720 1(7)	−0.229 0(7)	0.295 2(8)	C(4L)	0.873 8(6)	−0.028 1(6)	0.376 6(6)
C(32)	0.715 7(7)	−0.219 9(7)	0.117 9(8)	C(41L)	0.910 0(6)	−0.110 1(7)	0.401 8(7)
C(33)	0.823 6(7)	−0.111 3(7)	0.211 9(7)	C(42L)	0.872 2(7)	−0.163 8(7)	0.453 9(7)
C(41)	0.518 3(8)	−0.120 7(10)	0.320 0(9)	C(43L)	0.910 2(8)	−0.239 3(7)	0.481 9(8)
C(42)	0.442 3(8)	−0.058 8(9)	0.168 9(8)	C(44L)	0.985 4(8)	−0.257 4(8)	0.458 5(8)
C(43)	0.557 5(9)	−0.192 7(8)	0.169 8(8)	C(45L)	1.021 8(8)	−0.207 1(8)	0.405 9(10)
C(51)	0.743 5(7)	−0.030 8(7)	0.038 6(7)	C(46L)	0.985 7(7)	−0.131 4(8)	0.378 3(8)

(0.5 mm path length). Positive fast atom bombardment mass spectra were obtained using a Kratos MS50TC spectrometer, using CsI as calibrant. Proton NMR spectra were recorded in $CDCl_3$ using a Bruker 250 B MHz instrument, referenced to internal $SiMe_4$. The starting materials $[N(PPh_3)_2][Ru_5C(CO)_{14}]$, $[N(PPh_3)_2][Ru_6C(CO)_{16}]$[9] and $[\{Pd(\eta\text{-}C_4Ph_4)Cl\}_2]$[1] were prepared according to the literature procedures. Diphenylacetylene and $AgBF_4$ were purchased from Aldrich Chemicals.

Reaction of $[\{Pd(\eta\text{-}C_4Ph_4)Cl\}_2]$ with $AgBF_4$; *Preparation of* $[Pd(\eta\text{-}C_4Ph_4)(Me_2CO)_2][BF_4]_2$.—The complex $[\{Pd(\eta\text{-}C_4Ph_4)Cl\}_2]$ (*ca.* 100 mg), in acetone (20 cm^3) was treated with $AgBF_4$ (2.1 mol equiv.). The solution was stirred for 30 min after which it was filtered to remove AgCl which precipitates during the course of the reaction. The solvent was removed from the bright yellow filtrate and the resulting yellow-brown solid, $[Pd(\eta\text{-}C_4Ph_4)(Me_2CO)_2][BF_4]_2$, was obtained which was used *in situ* in the following reactions.

Reaction of $[N(PPh_3)_2][Ru_5C(CO)_{14}]$ *with* $[Pd(\eta\text{-}C_4Ph_4)(Me_2CO)_2][BF_4]_2$; *Preparation of* $[Ru_5C(CO)_{13}(\eta\text{-}C_4Ph_4)]$ **1**.—The cluster $[N(PPh_3)_2][Ru_5C(CO)_{14}]$ (150 mg) in dichloromethane (20 cm^3) was added dropwise to a solution of $[Pd(\eta\text{-}C_4Ph_4)(Me_2CO)_2][BF_4]_2$ (1.1 mol equiv.) in dichloromethane (20 cm^3) at reflux. The cluster was added over a 10 min period and the reaction mixture was stirred for a further 20 min. The solution was filtered through a short column containing silica gel using 50% dichloromethane–hexane as eluent and the dark brown solution was confirmed by spot TLC to comprise of one product only.

Spectroscopic data for the initial compound produced *i.e.* a precursor to **1** tentatively formulated as $[Ru_5PdC(CO)_{14}(\eta\text{-}C_4Ph_4)]$: ($\tilde{\nu}_{CO}/cm^{-1}$, CH_2Cl_2) 2060vs and 2027s. After standing for 24 h in dichloromethane the quantitative conversion of this precursor material takes place affording $[Ru_5C(CO)_{13}(\eta\text{-}C_4Ph_4)]$ **1** (80 mg). Spectroscopic data for **1**: $\tilde{\nu}_{CO}/cm^{-1}$ (CH_2Cl_2) 2080m, 2060s (sh), 2046vs, 2028s (sh), 1967w (br), 1906w (br) and 1792vw (br); ^1H NMR ($CDCl_3$) multiplet resonances are observed between δ 7.12 and 7.94; MS *m/z* 1237 M^+ (Calc. 1238) (Found: C, 41.35; H, 1.70. $C_{42}H_{20}O_{13}Ru_5$ requires C, 40.75; H, 1.65%).

Reaction of $[N(PPh_3)_2][Ru_6C(CO)_{16}]$ *with* $[Pd(\eta\text{-}C_4Ph_4)(Me_2CO)_2][BF_4]_2$; *Preparation of* $[Ru_6C(CO)_{15}(\eta\text{-}C_4Ph_4)]$ **2**.—The cluster $[N(PPh_3)_2][Ru_6C(CO)_{16}]$ (100 mg) in dichloromethane (20 cm^3) was added dropwise to a solution of $[Pd(\eta\text{-}C_4Ph_4)(Me_2CO)_2][BF_4]_2$ (1.1 mol equiv.) in dichloromethane (20 cm^3) at reflux. The cluster is added over a 10 min period and the reaction mixture was stirred for a further 20 min. The solution was filtered through a short column containing silica gel using 50% dichloromethane–hexane as eluent and the dark brown solution was confirmed by spot TLC to comprise of one product only which has been characterised as $[Ru_6C(CO)_{15}(\eta\text{-}C_4Ph_4)]$ **2**. Spectroscopic data for **2**: $\tilde{\nu}_{CO}/cm^{-1}$ (CH_2Cl_2) 2067s (sh), 2042vs, 2027s (sh), 1840m (br) and 1751w (br); ^1H NMR ($CDCl_3$) multiplet resonances are observed between δ 6.93 and 7.98; MS *m/z* 1395 M^+ (Calc. 1395) (Found: C, 38.95; H, 1.45. $C_{44}H_{20}O_{15}Ru_6$ requires C, 37.90; H, 1.45%).

Structural Characterisation.—Fractional atomic coordinates of **1** and **2** are given in Tables 1 and 2, respectively. Crystals of **1** were grown by slow evaporation from a dichloromethane–octane solution.

Crystal data. $C_{42}H_{20}O_{13}Ru_5$, M = 1237.93, monoclinic, space group $P2_1/c$ (no. 14), a = 16.604(6), b = 15.926(5), c = 15.743(4) Å, β = 95.39(6)°, U = 4145(2) $Å^3$ (by least-squares refinement of setting angles for 25 automatically centred reflections, λ = 0.710 73 Å), Z = 4, D_c = 1.984 g cm^{-3}, $F(000)$ = 2384. Red plate, crystal dimensions 0.07 × 0.27 × 0.62 mm, μ(Mo-Kα) = 1.845 mm^{-1}.

Data collection and processing. Enraf-Nonius CAD4 diffractometer operating at ambient temperature, ω–2θ scan mode with graphite monochromated Mo-Kα radiation. Three standard reflections were monitored every 100 reflections and showed no significant decomposition during the data collection

Table 2 Atomic coordinates with e.s.d.s in parentheses for **2**

Atom	*x*	*y*	*z*	Atom	*x*	*y*	*z*
Ru(1)	0.362 57(2)	0.728 35(2)	0.417 978(14)	C(43)	0.657 5(3)	0.698 6(2)	0.205 3(2)
Ru(2)	0.415 85(2)	0.939 86(2)	0.206 70(2)	C(61)	0.026 1(3)	0.846 3(2)	0.379 0(2)
Ru(3)	0.337 25(2)	0.940 14(2)	0.396 95(2)	C(62)	0.071 4(3)	0.957 6(2)	0.231 2(2)
Ru(4)	0.584 85(2)	0.791 73(2)	0.316 067(14)	C	0.383 8(3)	0.828 9(2)	0.306 6(2)
Ru(5)	0.460 14(2)	0.717 85(2)	0.221 61(2)	C(1L)	0.379 0(3)	0.674 6(2)	0.129 7(2)
Ru(6)	0.178 87(2)	0.885 08(2)	0.314 51(2)	C(11L)	0.267 3(3)	0.729 4(2)	0.083 1(2)
O(11)	0.503 5(3)	0.499 9(2)	0.404 4(2)	C(12L)	0.239 1(3)	0.830 7(2)	0.044 3(2)
O(12)	0.449 3(2)	0.720 0(2)	0.588 7(2)	C(13L)	0.134 5(4)	0.876 1(3)	−0.000 1(2)
O(13)	0.108 5(3)	0.680 6(2)	0.527 7(2)	C(14L)	0.055 1(4)	0.822 0(3)	−0.005 1(2)
O(21)	0.552 2(3)	0.871 6(2)	0.020 3(2)	C(15L)	0.081 9(4)	0.722 2(3)	0.032 3(3)
O(22)	0.197 6(3)	1.126 9(2)	0.139 5(2)	C(16L)	0.188 7(4)	0.675 2(3)	0.075 4(2)
O(23)	0.598 7(3)	1.067 0(2)	0.173 7(2)	C(2L)	0.529 8(3)	0.633 9(2)	0.101 0(2)
O(31)	0.596 8(2)	0.910 4(2)	0.455 6(2)	C(21L)	0.627 6(3)	0.634 3(2)	0.013 9(2)
O(32)	0.031 7(2)	1.075 1(2)	0.411 1(2)	C(22L)	0.766 3(3)	0.572 6(3)	0.004 1(2)
O(33)	0.233 0(2)	0.946 4(2)	0.599 7(2)	C(23L)	0.856 7(4)	0.568 1(3)	−0.079 3(2)
O(34)	0.325 1(3)	1.161 8(2)	0.358 7(2)	C(24L)	0.810 4(4)	0.623 0(3)	−0.154 4(2)
O(41)	0.837 7(3)	0.853 3(2)	0.227 1(2)	C(25L)	0.674 2(4)	0.683 4(3)	−0.145 9(2)
O(42)	0.730 3(2)	0.605 4(2)	0.430 3(2)	C(26L)	0.582 5(3)	0.689 5(2)	−0.062 4(2)
O(43)	0.766 7(2)	0.662 4(2)	0.160 5(2)	C(3L)	0.534 5(3)	0.561 7(2)	0.182 8(2)
O(61)	−0.069 6(2)	0.826 6(2)	0.415 8(2)	C(31L)	0.639 8(3)	0.461 2(2)	0.203 9(2)
O(62)	0.003 1(3)	1.001 9(2)	0.183 4(2)	C(32L)	0.634 6(4)	0.376 2(3)	0.175 8(2)
C(11)	0.451 7(3)	0.586 8(2)	0.402 2(2)	C(33L)	0.726 1(4)	0.278 3(3)	0.192 5(3)
C(12)	0.413 1(3)	0.722 6(2)	0.526 7(2)	C(34L)	0.825 8(4)	0.265 5(3)	0.236 4(3)
C(13)	0.198 6(3)	0.702 8(3)	0.484 7(2)	C(35L)	0.833 2(4)	0.349 8(3)	0.262 7(3)
C(21)	0.499 6(4)	0.883 8(3)	0.094 1(2)	C(36L)	0.740 3(3)	0.447 3(3)	0.247 7(2)
C(22)	0.276 9(3)	1.055 8(3)	0.164 5(2)	C(4L)	0.385 6(3)	0.599 1(2)	0.208 6(2)
C(23)	0.531 9(3)	1.018 9(3)	0.186 3(2)	C(41L)	0.280 7(3)	0.563 0(2)	0.272 4(2)
C(31)	0.535 6(3)	0.894 6(2)	0.414 9(2)	C(42L)	0.312 4(3)	0.463 2(2)	0.314 8(2)
C(32)	0.124 3(3)	1.003 5(2)	0.385 9(2)	C(43L)	0.209 5(4)	0.428 3(3)	0.370 0(2)
C(33)	0.269 6(3)	0.943 8(2)	0.524 5(2)	C(44L)	0.074 6(4)	0.492 2(3)	0.384 0(2)
C(34)	0.331 4(3)	1.078 5(2)	0.371 9(2)	C(45L)	0.041 7(4)	0.591 8(3)	0.342 8(3)
C(41)	0.742 6(3)	0.832 6(3)	0.259 3(2)	C(46L)	0.143 1(3)	0.626 9(2)	0.287 9(2)
C(42)	0.676 2(3)	0.676 6(2)	0.389 2(2)				

period. Absorption corrections were applied by the use of semi-empirical ψ-scans. A total of 5334 reflections were measured ($2.6 < \theta < 22.5°$, $+h, +k, \pm l$) and averaged to yield 5121 unique reflections (merging $R_{int} = 0.0486$) of which 3737 have $F_o > 4\sigma(F_o)$. Corrections for Lorentz and polarisation effects were applied.

Structure analysis and refinement. Structure solution involved a combination of direct methods and Fourier techniques. Hydrogen atoms were placed in calculated positions and refined using a riding model. Anisotropic thermal motion was assumed for all non-hydrogen atoms. Full-matrix least-squares refinement on F_o^2 for 5121 data and 541 parameters converged to $wR_2 = 0.1249$ (all data) where $wR_2 = \{\Sigma[w(F_o^2 - F_c^2)^2]/\sigma[w(F_o^2)^2]\}^{\frac{1}{2}}$, conventional $R_1 = 0.0473$ (observed data) where $R_1 = \Sigma||F_o| - |F_c||/\Sigma|F_o|$, $(\Delta/\sigma)_{max} = 0.001$, goodness-of-fit = 1.027. The function minimised was $\Sigma w(F_o^2 - F_c^2)^2$, $w = 1/[\sigma^2(F_o^2) + (0.0635P)^2 + 11.7873P]$ where $P = (F_o^2 + 2F_c^2)/3$ and σ was obtained from counting statistics. A final difference electron density Fourier synthesis revealed maximum and minimum residual electron density peaks of 2.36 and −0.95 e Å^{-3}, which were located in close proximity to ruthenium atom positions.

Crystals of **2** were grown by slow evaporation from a dichloromethane–octane solution.

Crystal data. $C_{44}H_{20}O_{15}Ru_6$, $M = 1395.02$, triclinic, space group $P\bar{1}$(no. 2), $a = 10.887(4)$, $b = 14.183(5)$, $c = 15.674(6)$ Å, $\alpha = 78.43(2)$, $\beta = 72.99(2)$, $\gamma = 67.42(2)°$, $U = 2126(13)$ Å^3 (by least-squares refinement of 2θ values for 32 automatically centred reflections, $\lambda = 0.710\,73$ Å), $Z = 2$, $D_c = 2.179$ g cm^{-3}, $F(000) = 1336$. Red blocks, crystal dimensions 0.19 × 0.35 × 0.47 mm, μ(Mo-Kα) = 2.149 mm^{-1}.

Data collection and processing. Stoë Stadi-4 diffractometer operating at 150 K, ω–2θ scan mode with graphite-monochromated Mo-Kα radiation. Three standard reflections were monitored every 60 min and showed no significant decomposition during the data collection. Absorption corrections were applied by the use of semi-empirical ψ-scans. A total of 9750 reflections were measured ($2.7 < \theta < 27.5°$, $\pm h, \pm k, \pm l$) and averaged to yield 9748 unique reflections [merging $R_{int} = 0.0619$] of which 8912 have $F_o > 4\sigma(F_o)$. Corrections for Lorentz and polarisation effects were applied.

Table 3 Parameters used in extended-Hückel calculations

Atom	Orbital	H_{ii}/eV	ζ_1
H	1s	−13.60	1.300
C	2s	−21.40	1.625
C	2p	−11.40	1.625
O	2s	−32.30	2.275
O	2p	−14.80	2.275
Ru*	4d	−12.39	4.210
Ru	5s	−9.16	2.078
Ru	5p	−4.78	2.043

* $\zeta_2 = 1.950$, $C_1 = 0.5772$, $C_2 = 0.5692$.

Structure analysis and refinement. Structure solution involved a combination of direct methods and Fourier techniques. Hydrogen atoms were placed in calculated positions and refined using a riding model. Anisotropic thermal motion was assumed for all non-hydrogen atoms. Full-matrix least-squares refinement on F_o^2 for 9740 data and 587 parameters converged to $wR_2 = 0.0645$ (all data), conventional $R_1 = 0.0256$ (observed data), $(\Delta/\sigma)_{max} = 0.004$, goodness-of-fit = 1.152. The function minimised was $\Sigma w(F_o^2 - F_c^2)^2$, $w = 1/[\sigma^2(F_o^2) + (0.0279P)^2 + 2.5967P]$ where $P = (F_o^2 + 2F_c^2)/3$ and σ was obtained from counting statistics. A final difference electron density Fourier synthesis revealed maximum and minimum residual electron density peaks of 0.63 and −0.73 e Å^{-3}, which were located in close proximity to ruthenium atom positions.

For both structural analyses computations were performed

with the SHELXTL-PC[10] package and SHELXL 93[11] program.

Additional material available from the Cambridge Crystallographic Data Centre comprises H-atom coordinates, thermal parameters and remaining bond lengths and angles.

Extended-Hückel Calculations.—The extended-Hückel calculations[12] described in this work were done using the CACAO program.[13] Parameters used are shown in Table 3. The Ru–Ru distances were fixed at 2.90 Å, Ru–CO at 2.10 Å, CO at 1.14 Å, Ru–C(C_4H_4) at 2.20 Å and C–H at 1.01 Å.

Acknowledgements

We thank the EPSRC and NATO for financial support.

References

1 P. M. Maitlis and M. L. Games, *J. Am. Chem. Soc.*, 1963, **85**, 1887.
2 D. F. Pollock and P. M. Maitlis, *J. Organomet. Chem.*, 1971, **26**, 407.
3 H. Wadepohl, *Angew. Chem., Int. Ed. Engl.*, 1992, **31**, 247; D. Braga, P. J. Dyson, F. Grepioni and B. F. G. Johnson, *Chem. Rev.*, 1994, **94**, 1585.
4 P. J. Bailey, A. J. Blake, P. J. Dyson, S. L. Scott and B. F. G. Johnson, *J. Chem. Soc., Chem. Commun.*, 1994, 2233.
5 A. J. Blomquist and P. M. Maitlis, *J. Am. Chem. Soc.*, 1962, **84**, 2329.
6 M. P. Gomez-Sal, B. F. G. Johnson, J. Lewis, P. R. Raithby and A. H. Wright, *J. Chem. Soc., Chem. Commun.*, 1993, 9062.
7 D. H. Farrar, A. J. Poë and Y. Zheng, *J. Am. Chem. Soc.*, 1994, **116**, 6252; D. B. Brown, P. J. Dyson, B. F. G. Johnson and D. Parker, *J. Organomet. Chem.*, 1995, **491**, 189.
8 B. F. G. Johnson, J. Lewis, J. N. Nicholls, J. Puga, P. R. Raithby, M. J. Rosales, M. McPartlin and W. Clegg, *J. Chem. Soc., Dalton Trans.*, 1983, 277.
9 D. Braga, F. Grepioni, P. J. Dyson, B. F. G. Johnson, P. Frediani, M. Bianchi and F. Piacenti, *J. Chem. Soc., Dalton Trans.*, 1992, 2565.
10 G. M. Sheldrick, SHELXTL-PC, release 4.4, Siemens Analytical X-Ray Instruments Inc., Madison, WI, 1992.
11 G. M. Sheldrick, SHELXL 93, Program for structure refinement, University of Göttingen, 1993.
12 R. Hoffmann and W. N. Lipscomb, *J. Chem. Phys.*, 1962, **36**, 2179; 1963, **37**, 2872.
13 C. Mealli and D. E. Prosperpio, *J. Chem. Educ.*, 1990, **67**, 399.

Received 23*rd March* 1995; *Paper* 5/01879J